metals

MDPI

Article

Effect of SiO_2 on the Mechanical Property and Reduction of Calcium Ferrite

Daiwei Yang [1], Wei Wang [1,2,*], Runsheng Xu [1,*], Jingxuan Li [2] and Mingming Song [2]

[1] State Key Laboratory of Refractories and Metallurgy, Wuhan University of Science and Technology, Wuhan 430081, China; 18140683241@163.com

[2] Key Laboratory for Ferrous Metallurgy and Resources Utilization of Ministry of Education, Wuhan University of Science and Technology, Wuhan 430081, China; 15855419894@163.com (J.L.); smma987@163.com (M.S.)

* Correspondence: wangwei74@wust.edu.cn (W.W.); xu_runsheng@163.com (R.X.); Tel.: 02768862651 (W.W. and R.X.)

Received: 28 November 2018; Accepted: 24 January 2019; Published: 29 January 2019

Abstract: SiO_2-Fe_2O_3-CaO (SFC) is believed to be the transition phase during the SiO_2-Fe_2O_3-CaO-Al_2O_3 (SFCA) formation process. The effect of SiO_2 on the mechanical property and reduction of the CaO-Fe_2O_3-SiO_2 system was inspected in this study. Experiments were carried out under air at 1200 °C with different amounts of SiO_2 mixed with Fe_2O_3 and CaO. The mechanical properties and reduction of samples were studied. Results indicate that the hardness of samples gradually increases with the increase of SFC content. That may be caused by SiO_2 solid solution in calcium ferrite. The larger the amount and smaller size of acicular calcium ferrites in samples, the greater the fracture toughness. The solid solution of SiO_2 in calcium ferrite is beneficial to decrease the initial reduction temperature. The apparent activation energy values of the samples with the different content of SiO_2 from 0% to 5% are 167.23, 84.36, 87.90, 96.02, 92.44 and 107.83 kJ·mol^{-1}, respectively. The microstructure of lump samples after reduction consists of four phases, i.e., CF ($CaFe_2O_4$), SFC, calcio-wüstite (CW) and Fe. It was not difficult to find the Fe in the samples reduced from CW. Scanning electron micrograph images have revealed that the acicular-like calcium ferrites are more easily reduced than the platy-like ones.

Keywords: calcium ferrite; SiO_2; microstructure; mechanical property; reduction reaction

1. Introduction

Under the pressures of the decreases of high-quality iron ore, the iron and steel enterprises in China turn to use low-quality ores. The SFCA phase (SiO_2-Fe_2O_3-CaO-Al_2O_3) is regarded as a desirable bonding phase for fluxed sinter [1,2]. Silica content influences the phase composition and bonding phase mass of SFCA because of their low melting point [3,4], high mechanical strength [5–8], and SFCA is an important part of the point of view of saving cost and energy from low temperature sinter. SiO_2-Fe_2O_3-CaO (SFC) is believed to be the transition phase during the SFCA formation process and has been widely investigated [9–11].

SFCA mechanical properties of calcium ferrite with different morphologies and content vary greatly. Compared with grained or plate-like calcium ferrite, fine acicular calcium ferrite has higher microhardness, and it can prevent crack extension effectively. That makes acicular calcium ferrite better the compressive strength and metallurgical properties than grained or plate-like calcium ferrite [12,13]. Many researchers considered that SiO_2 and Al_2O_3 were necessary components for the formation of acicular calcium ferrite [14,15]. Furthermore, acicular calcium ferrite can also enable the better reduction of sinter. Murakami T et al. [12] found that the reduction of columnar calcium

ferrite in sinter was worse than that of acicular calcium ferrite. It seems that the diffusion of the reducing gas is difficult compared with the case of acicular calcium ferrite coexisted with small pores. Cai B et al. [16] SFCA phases in 'Acicular SFCA' have fine pores around them. It is significant to study the effect of silico and aluminum on the mechanical property and reduction mechanism of calcium ferrite. The reduction of powdered samples under isothermal conditions research of ternary calcium ferrite of CaO-Fe_2O_3-x system (x: SiO_2, Al_2O_3) have been further investigated by Ding C et al. [17,18], but it is still not comprehensive enough, and more research on different aspects is needed.

In this paper, the effect of SiO_2 on the mechanical property and reduction of calcium ferrite will be investigated. Specifically, we include the following methods: the samples of hardness and fracture toughness test, powder non-isothermal reduction and block isothermal reduction. This will contribute to more deeply understanding the effect of SiO_2 on the properties of calcium ferrite and sinter.

2. Experimental Materials and Methods

2.1. Materials

The samples were prepared from Fe_2O_3 ($w(Fe_2O_3)$ ≥ 99.99%), SiO_2 ($w(SiO_2)$ ≥ 99.99%) and $Ca(OH)_2$ ($w(Ca(OH)_2)$ ≥ 99.99%). In order to assure that the main formed phase is $CaO{\cdot}Fe_2O_3$ in the samples, the mole ratio of $Ca(OH)_2$ and Fe_2O_3 is 1:1. Fe_2O_3, $Ca(OH)_2$ and SiO_2 were added according to the mass ratio in Table 1. The samples were pressed into briquettes size of Φ 20 mm × 20 mm using a briquetting machine at a pressure of 5.0 MPa for nearly 1 min. Subsequently, prepared sample was placed into an alumina crucible. Then the sintering experiment was carried out in a muffle furnace (SX2-10-13, Experimental electric furnace factory, Changsha, China). The sintering temperature raised from room temperature to 1200 °C (1473 K) at 10 °C/min (10 K/min), held for 8 h to react completely. Finally, sintered samples were cooled down in the air. X-ray diffraction (XRD, X'Pert PRO MPD, PANalytical Co. Ltd., Almelo, Netherlands) analysis was conducted to confirm the phase composition of the roasted samples. Scanning was carried out at an angular range from 10° to 90° and scan rate of 5°/min, the test results are shown in Figure 1.

Table 1. The composition of samples.

Sample Number	w(CaO) %	$w(Fe_2O_3)$ %	$w(SiO_2)$ %
1	25.9	74.1	0.0
2	25.7	73.3	1.0
3	25.4	72.6	2.0
4	25.1	71.9	3.0
5	24.9	71.1	4.0
6	24.6	70.4	5.0

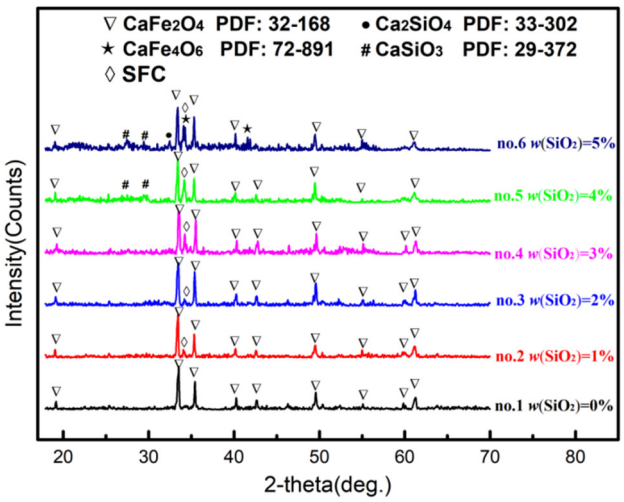

Figure 1. XRD analysis of the powdered samples with different of SiO_2 mass fractions at 1200 °C.

2.2. Mechanics and Reduction Experiments

Hardness of samples was tested by HV1000B micro Vickers hardness tester (Xinyun Co., Ltd., Hebi, China) and was reported as standard Vickers hardness number (Hv). Polished sinter samples were used for this study. Standard indentation procedures were employed throughout, and a load of 981 mN was used for all the phases. The indentation time was kept constant at 10 s. The *H* (Microhardness) is determined based on the average of 10 data points for each phase by Vickers. *E* (Modulus of Elasticity) and K_{IC} (Fracture toughness) were defined as follows by Knoop indentation [19].

$$K_{IC} = \delta\left(\frac{E}{H}\right)^{1/2}\frac{P}{c^{3/2}}, \quad (1)$$

where δ (δ = 0.0153) is material independent constant, *P* is the applied load pressure, *c* is crack length.

$$\frac{b}{a} = \frac{1}{7.11} - \alpha\frac{H}{E}, \quad (2)$$

where the ratio of the diagonal dimensions of the Knoop head is defined by the indenter geometry 7.11, and *a*/*b* is impression long and short diagonal ratio and α (α = 0.45) is using a gradient adjusted to fit the data.

TG measurement of the reduction of samples was conducted using a microcomputer differential thermal balance (HCT-3, Henven Scientific Instrument Factory, Beijing, China). Powdered samples (20 mg) were heated at heating rate of 10 K/min from room temperature to 1100 °C (1373 K) with 50 ml/min mix gas (30% CO and 70% N_2). Lump samples (160 ± 0.5 mg) were placed in an alumina crucible (Φ 7 mm ×1.5 mm) and were heated at heating rate of 10 K/min from room temperature to 700 °C (973 K) in alumina crucible with 50 ml/min 100% N_2 atmosphere. Then, it was held for 60 min at 50 ml/min mix gas (30% CO and 70% N_2) at 700 °C (973 K). Finally, the morphology of reacted lumpy sample was observed using scanning electron microscopy (EVO-MA10, SEM Zeiss, Oberkochen, Germany).

2. Results and Discussion

3.1. Effect of SiO_2 on the Mechanical Properties of Calcium Ferrite

The morphologies of samples with different SiO_2 contents at 1200 °C are shown in Figure 2. The content of SiO_2 has great influence on the morphology of mineral phases in sintered samples. The morphology of calcium ferrite in sample no.1 is mainly grained. The grained calcium ferrites are gradually transformed into the column or acicular calcium ferrites with SiO_2 added, as shown in samples no.1 to samples nos.2 and 3. With the content of SiO_2 increasing, the sizes of calcium ferrites gradually become smaller.

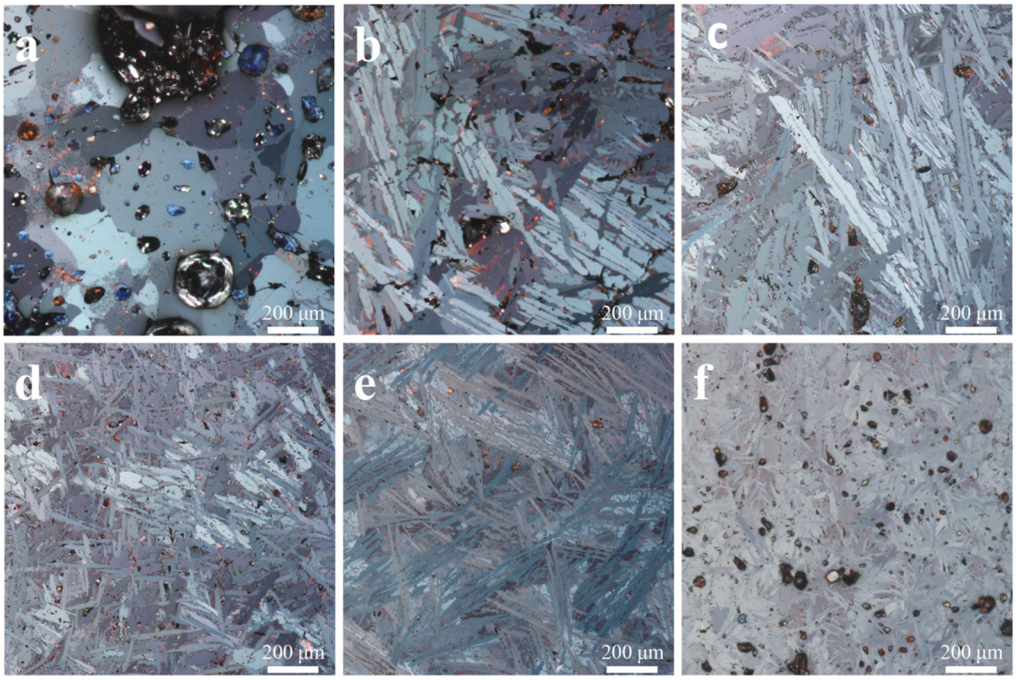

Figure 2. Morphology of samples with different of SiO_2 mass fraction: (**a**) sample no.1 $w(SiO_2)$ = 0%; (**b**) sample no.2 $w(SiO_2)$ = 1%; (**c**) sample no.3 $w(SiO_2)$ = 2%; (**d**) sample no.4 $w(SiO_2)$ = 3%; (**e**) sample no.5 $w(SiO_2)$ = 4%; (**f**) sample no.6 $w(SiO_2)$ = 5%.

Vickers hardness of samples with the different content of SiO_2 were measured. The experimental results are shown in Table 2. The Vickers hardness and fracture toughness of the samples increased first and then decreased with the increase of SiO_2 content at 1200 °C. Combined with XRD analysis, the Vickers hardness in the sample increases with the increase of SFC diffraction peak strength. It indicates that SiO_2 solid solution in calcium ferrite forms SFC. It is helpful to increase the hardness. From Figure 2 and Table 2, it is possible to find that the size of acicular calcium ferrite is smaller with the content SiO_2 increasing, and the greater the fracture toughness. However, when $w(SiO_2)$ > 4%, a small amount of silicate with high melting point and low strength was formed and the hardness and the fracture toughness of the sample decreased obviously.

Table 2. Vickers hardness of calcium ferrites with different SiO_2 content.

Samples	H_V/Gg·m^{-2}		K_{IC}/ (MN·m$^{-2/3}$)
	Range of Measurement	Average of Measurement	
1	490.8–623.3	578.7	0.94
2	567.7–747.5	681.7	1.36
3	639.4–762.8	716.3	1.39
4	686.3–890.3	758.8	1.56
5	633.5–744.8	681.8	2.10
6	600.2–710.9	658.8	1.83

3.2. Effect of SiO_2 on the Reduction of Calcium Ferrite

3.2.1. Reduction Kinetic Analysis of Powder Sample

The reduction conversion was calculated by mass loss of samples. Reduction degree (x) can be described as follows [20,21]:

$$x = \frac{m_0 - m_t}{m_0 - m_\infty}, \tag{3}$$

where m_0 is the samples mass at the start of reduction, mg; m_t is the samples mass at reduction time of t, mg; m_∞ is the theoretical sample mass assuming full reduction of iron oxide (s) contained in the sample, mg. The m_∞ of samples no.1 to no.6 are 4.44, 4.40, 4.35, 4.31,4.27 and 4.22 mg in this paper. The reduction route of CF is described as follows:

$$CF \rightarrow CWF + C_2F \rightarrow CW_3F + C_2F \rightarrow C_2F \rightarrow Fe$$

The mass loss rate of samples sintered during reduction is a function of reaction time and temperature, and it can be expressed as [22,23]:

$$\frac{dx}{dt} = k(T)f(x), \tag{4}$$

$\frac{dx}{dt}$ is the mass loss rate, s^{-1}, $k(T)$ is the rate constant, which is a function of temperature; $f(x)$ is the differential form of the reaction mechanism function; t is the reaction time, s; x is the reaction conversion.

According to the Arrhenius equation shown in Equation (5):

$$k = A\exp(-\frac{E}{RT}), \tag{5}$$

where A is the pre-exponential factor, which contributes to the reaction rate, s^{-1}; E is the activation energy, $kJ \cdot mol^{-1}$; R is the standard molar gas constant, $kJ \cdot mol^{-1} \cdot K^{-1}$.

During a non-isothermal process, the heating rate β ($°C \cdot s^{-1}$) is constant:

$$\beta = \frac{dT}{dt}, \tag{6}$$

The following formula can be obtained from Equations (4) and (6):

$$\frac{dx}{dT} = \frac{A}{B}\exp(-\frac{E}{RT})f(x), \tag{7}$$

Equation (5) can be integrated to give:

$$G(x) = \int_0^x \frac{dx}{f(x)} = \frac{A}{\beta}\int_0^T \exp(-\frac{E}{RT})dT, \tag{8}$$

The following Equations (7) and (8) can be obtained by approximate calculation:

$$\frac{A}{B}\int_0^T \exp(-\frac{E}{RT})dT \cong \frac{ART^2}{\beta E}(1-\frac{2RT}{E})\exp(-\frac{E}{RT}), \tag{9}$$

$$1-\frac{2RT}{E} \cong 1. \tag{10}$$

The following formula can be obtained from Equations (9) and (10):

$$\ln\left[\frac{G(x)}{T^2}\right] = \ln\left(\frac{AR}{\beta E}\right) - \frac{E}{RT}. \quad (11)$$

Model function $G(x)$ was obtained to describe the relationship of reaction degree with time. Eight normal functions expressing the solid-state reaction are listed in Table 3 [24,25,26].

Table 3. Model function $G(x)$ for normal solid-state reactions.

Symbol	Kinetic Models	Code	$G(x)$
Reaction-order	Instantaneous nucleation and unidimensional growth	F1	$-\ln(1-x)$
Diffusion models	One-dimensional diffusion	D1	x^2
	Two-dimensional diffusion cylindrical symmetry	D2	$x + (1-x)\ln(1-x)$
	Three-dimensional diffusion spherical symmetry, $N = 3$	D3	$[1-(1-x)^{1/3}]^2$
	Three-dimensional diffusion cylindrical symmetry	D4	$(1-2/3x) - (1-x)^{2/3}$
Geometrical contraction	Phase boundary reaction, cylindrical symmetry, $N = 1/2$	R2	$1-(1-x)^{1/2}$
	Phase boundary reaction, spherical symmetry, $N = 1/3$	R3	$1-(1-x)^{1/3}$
Nucleation models	Random nucleation and subsequent growth, $N = 1/2$, $M = 2$	A2	$[-\ln(1-x)]^{1/2}$
	Random nucleation and subsequent growth, $N = 1/3$, $M = 3$	A3	$[-\ln(1-x)]^{1/3}$

The relationship between reduction degree and temperature of powdered samples with different SiO_2 content is shown in Figure 3. The maximum reduction degree and its corresponding time for samples are shown in Table 4, where x_m, T_i and T_f [27] are the maximum reduction degree, initial mass loss temperature and maximum mass loss temperature of reduction reaction, respectively. With the increase of SiO_2 content, the initial reduction temperature decreases gradually, and when $w(SiO_2)$ content exceeds 3%, the initial reduction temperature is stable (508.6–510.6 °C). The formation and increasing of SFC by solid solution of SiO_2 in CF are beneficial to decrease the initial reaction temperature.

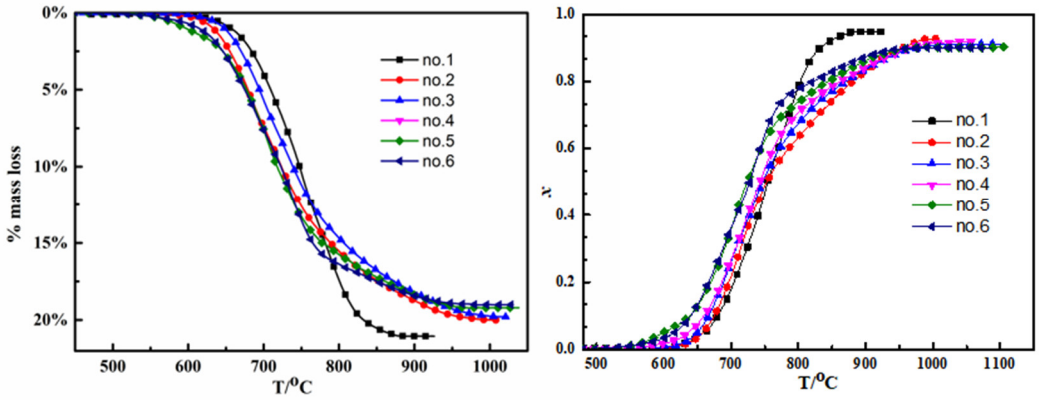

Figure 3. % mass loss versus temperature (**a**) and reduction degree versus reaction temperature (**b**).

Table 4. Initial and terminational temperature of reduction reaction of samples.

Samples	x_m	T_i/°C	T_f/°C
1	0.947	588.4	875.4
2	0.925	578.8	987.1
3	0.910	569.5	1035.2
4	0.918	546.5	1047.0
5	0.902	510.6	991.0
6	0.900	508.6	980.2

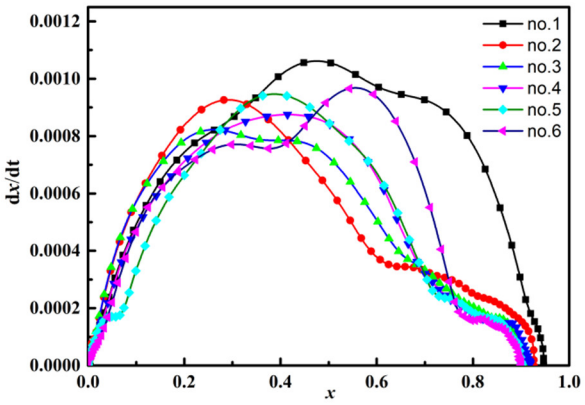

Figure 4. Reduction rate dx/dt vs. reduction degree α for the reduction.

The relationship between reduction degree and reduction rate of powdered samples with different SiO_2 content by non-isothermal thermal analysis is shown in Figure 4. It can be seen from Figure. 3 that when x was over 0.6, the reduction rate of sample 1 was much higher than that of sample 2, although the reduction temperature of sample 1 was lower than that of the rest of samples. This may be due to the fact that there are $FeO{\cdot}SiO_2$ or $CaO{\cdot}FeO{\cdot}SiO_2$ during the reduction process, which is difficult to reduce. The reduction termination temperature of the samples was increased. The fitting lines for the reaction of samples and kinetic parameters are shown in Figure 5 and Table 5, respectively. R is the correlation coefficient, and the larger the R, the better correlation of the mechanism function. It can be seen that the best fittings for all samples are those of F1. The apparent activation energy values of all samples are 167.23, 84.36, 87.90, 96.02, 92.44 and 107.83 $kJ{\cdot}mol^{-1}$. Sample reduction tends to be easy with the addition of SiO_2 in the Fe_2O_3-CaO system. Moreover, the reduction of sample No. 2 is the most easily activated among all the samples.

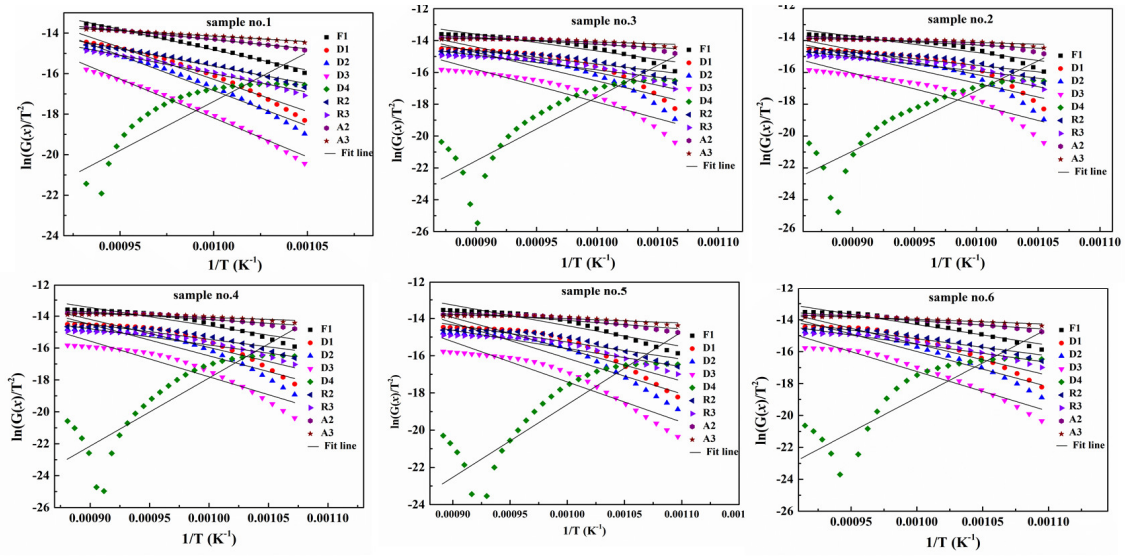

Figure 5. Reduction kinetic calculation of samples with different SiO_2 content.

Table 5. Kinetic parameters fitted by different mechanism function.

Samples	The Best Mechanism Functions	E/(kJ·mol^{-1})	A/s^{-1}	R^2
1	F1	167.23	663514.90	0.995
2	F1	84.36	17.02	0.882
3	F1	87.90	29.36	0.899
4	F1	96.02	89.62	0.910
5	F1	92.44	70.23	0.903
6	F1	107.83	568.32	0.952

3.2.2. Reduction Analysis of Lump Sample

Figure. 6 shows the changes in mass loss of samples with different content of SiO_2 at 700 °C, under max gas (30%CO and 70%N_2). The main factors affecting the reduction of lump samples are porosity, phase composition and morphology. The number of holes at sample no.1 which belongs to solid sintering, is obviously higher than that of the other samples. The mass loss of the rest of lump samples increases gradually with the increase of SiO_2 content. As shown in Figure 2, there was no obvious difference in the number of holes for samples 2–5. It conduced that the mass loss of sample no.1 was obviously higher than that of other samples. The difference of mass loss of samples no.2 and no.3 was not particularly large. This was consistent with the difference of the morphology and the activation energy between samples no.2 and no.3. Although the activation energy of the powder sample no.4 is higher than that of sample no.3, the rate of lump sample no.4 reduction is obviously higher than that of no.3. The reductions of calcium ferrite in these samples are greatly affected by the morphology. In other words, the finer acicular calcium ferrite helps to increase the reduction rate.

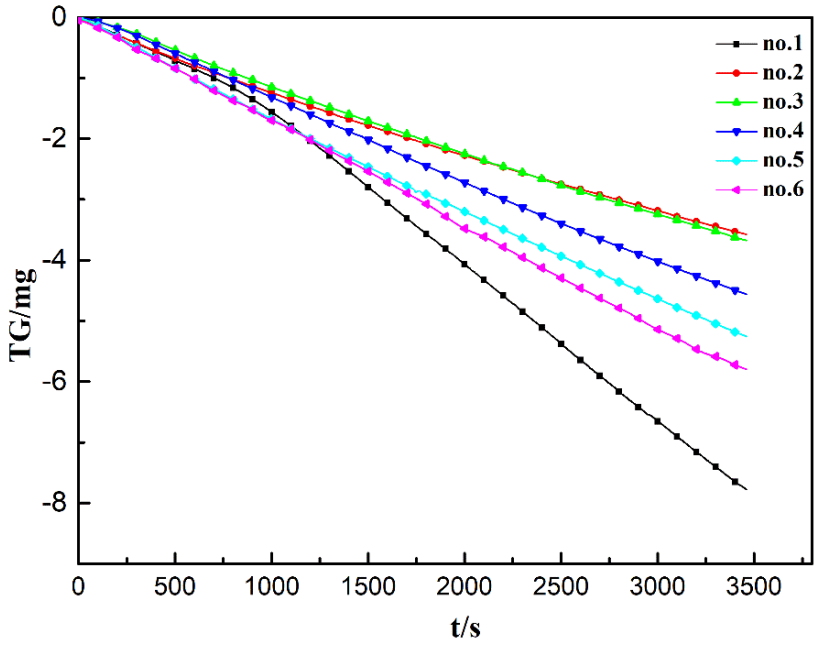

Figure 6. Experimental weightlessness curves of different lump samples with different SiO_2 content.

The morphologies of the samples after reduction, with $w(SiO_2)$ values ranging from 0 to 5%, were observed as shown in Figure 7. The microstructure in Figure 7 consists of four phases, i.e., calcium ferrite (CF), SFC, calcio–wüstite (CW) reduced from CF and SFC, Fe. The element compositions of the phases in these samples are listed in Table 6. It was not difficult to find the samples were reduced to Fe via CW. There are mainly Fe near acicular calcium ferrites and the pore in Figure 7. Most of the newly formed iron is acicular calcium ferrite in samples no.2–6. Therefore, it can be concluded that the acicular calcium ferrites are more easily reduced than the platy-like calcium ferrite.

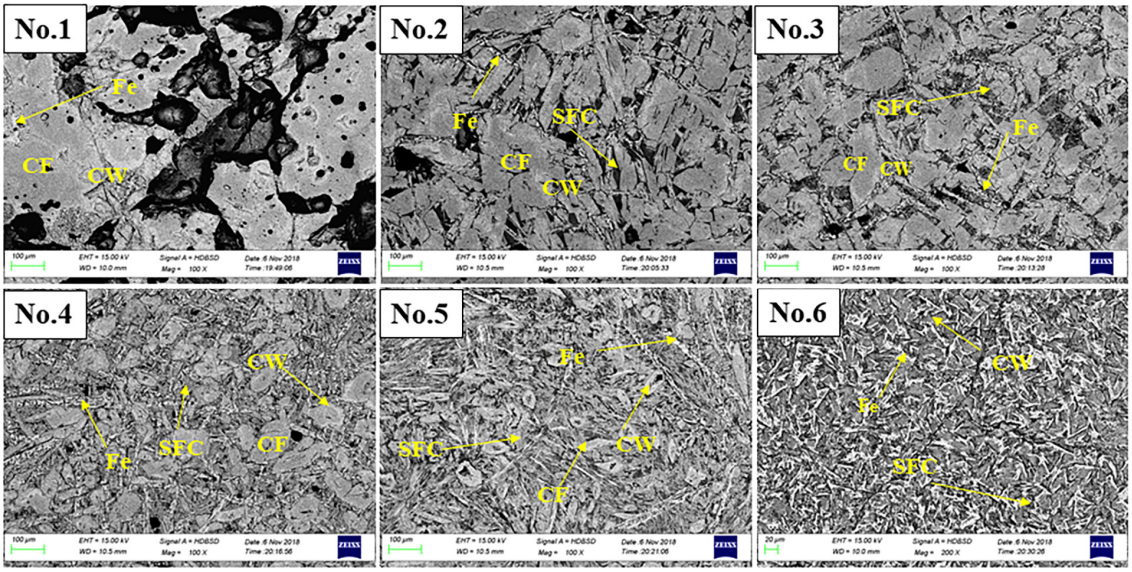

Figure 7. Phase morphology of sample nos. 1–6 after reduction at 700 °C (CF: $CaFe_2O_4$, CW: calcio–wüstite).

Table 6. EDS analysis results of the samples after reduction, in atomic %.

Sample Number		Elements			
		Fe	O	Ca	Si
no.1	CF	29.07	55.85	15.08	0.00
	CW	39.10	43.76	17.15	0.00
	Fe	89.97	6.02	4.01	0.00
no.2	CF	29.59	55.13	15.28	0.00
	CW	35.39	46.88	17.72	0.00
	Fe	63.33	27.94	8.57	0.14
	SFC	24.10	54.98	16.72	3.67
no.3	CF	28.43	54.76	16.80	0.00
	CW	35.93	51.52	12.43	0.10
	Fe	57.18	21.69	20.97	0.14
	SFC	21.52	62.11	13.16	2.82
no.4	CF	26.33	58.08	15.59	0.00
	CW	37.01	50.63	12.24	0.11
	Fe	84.60	8.05	7.35	0.00
	SFC	19.59	62.53	13.16	4.13
no.5	CF	29.59	55.13	15.28	0.00
	CW	36.93	50.60	12.23	0.21
	Fe	58.81	23.29	13.87	3.52
	SFC	20.98	59.03	16.70	2.88
no.6	CW	40.79	47.44	11.77	0.00
	Fe	53.95	37.42	8.62	0.00
	SFC	33.31	47.02	16.78	2.53

4. Conclusions

This was a fundamental study of the effect of SiO_2 on the mechanical property and reduction mechanism of calcium ferrite in iron ore sinter. Obtained results are summarized as follows.

Results indicate that SFC with SiO_2 solid solution in calcium ferrite forms is helpful in increasing hardness. With the content of SiO_2 increasing, the size of calcium ferrites gradually becomes smaller. The size of ACF is smaller with the content SiO_2 increasing, and the greater the fracture toughness.

The SiO_2 in CF is beneficial to decrease the initial reaction temperature and the apparent activation energies of reduction. The reduction termination temperature of the sample is also increased with the SiO_2 addition. The apparent activation energy values of the samples with the different content of SiO_2 from 0% to 5% are 167.23, 84.36, 87.90, 96.02, 92.44 and 107.83 $kJ \cdot mol^{-1}$, respectively.

The finer acicular calcium ferrite helps to increase the reduction rate. The samples were reduced to Fe from calcio–wüstite (CW) and most of the Fe was near acicular calcium ferrites and the pore rather than the platy calcium ferrites. This indicatea that the acicular-like calcium ferrites are more easily reduced than the platy-like ones.

Author Contributions: W.W., R.X. and D.Y. conceived and designed the experiments; D.Y. and J.L. performed the experiments; W.W. and D.Y. analysed the data and wrote the original manuscript; M.S. and R.X. reviewed and corrected the paper.

Funding: This research was funded by the National Natural Science Foundation of China grant number 51474164, 51704216, U1760101.

Acknowledgments: The authors acknowledge financial support from the National Natural Science Foundation of China (51474164, 51704216, U1760101).

Conflicts of Interest: The authors declare no conflicts of interest.

References.

1. Fernández-González, D.; Ruiz-Bustinza, I.; Mochón, J.; González-Gasca, C.; Verdeja, L.F. Iron ore sintering: Process. *Miner. Proc. Extr. Metall. Rev.* **2017**, *38*, 215–227, doi:10.1080/08827508.2017.1288115.
2. Fernández-González, D.; Ruiz-Bustinza, I.; Mochón, J.; González-Gasca, C.; Verdeja, L.F. Iron ore sintering: Quality Indices. *Miner. Proc. Extr. Metall. Rev.* **2017**, *38*, 254–264, doi:10.1080/08827508.2017.1323744.
3. Webster, N.A.S.; Pownceby, M.I.; Madsen, I.C. In situ X-ray Diffraction Investigation of the Formation Mechanisms of Silico-Ferrite of Calcium and Aluminium-I-type (SFCA-I-type) Complex Calcium Ferrites. *ISIJ Int.* **2013**, *53*, 1334–1340, doi:10.2355/isijinternational.53.1334.
4. Webster, N.A.S.; O'Dea, D.P.; Ellis, B.G.; Pownceby, M.I. Effects of Gibbsite, Kaolinite and Al-rich Goethite as Alumina Sources on Silico-Ferrite of Calcium and Aluminium (SFCA) and SFCA-I Iron Ore Sinter Bonding Phase Formation. *ISIJ Int.* **2017**, *57*, 41–47, doi:10.2355/isijinternational.ISIJINT-2016-332.
5. Sinha, M.; Ramna, R.V. Effect of Variation of Alumina on the Microhardness of Iron Ore Sinter Phases. *ISIJ Int.* **2009**, *49*, 719–721, doi:10.2355/isijinternational.49.719.
6. Zhou, M.; Yang, S.T.; Jiang, T.; Xue, X.X. Influence of MgO in form of magnesite on properties and mineralogy of high chromium, vanadium, titanium magnetite sinters. *Ironmak. Steelmak.* **2015**, *42*, 217–225, doi:10.1179/1743281214y.0000000223.
7. Sinha, M.; Nistala, S.H.; Chandra, S.; Mankhand, T.R.; Ghose, A.K. Correlating mechanical properties of sinter phases with their chemistry and its effect on sinter quality. *Ironmak. Steelmak.* **2017**, *44*, 100–107, doi:10.1080/03019233.2016.1226004.
8. Loo, C.E.; Wan, K.T.; Howes, V.R. Mechanical properties of natural and synthetic mineral phases in sinters having varying reduction degradation indices. *Ironmak. Steelmak.* **1988**, *15*, 279–285.
9. Ding, X.; Guo, X.-M. The Formation Process of Silico-Ferrite of Calcium (SFC) from Binary Calcium Ferrite. *Metall. Mater. Trans. B-Process Metall. Mater. Proc. Sci.* **2014**, *45*, 1221–1231, doi:10.1007/s11663-014-0041-z.
10. Ding, X.; Guo, X.-M. The Sintering Characteristics of Mixing SiO_2 with Calcium Ferrite at 1473 K (1200 degrees C). *Metall. Mater. Trans. B-Process Metall. Mater. Proc. Sci.* **2015**, *46*, 1742–1750, doi:10.1007/s11663-015-0348-4.

11. Ding, X.; Guo, X.-M.; Ma, C.-Y.; Tang, K.; Zhao, Y.-D. Effect of SiO_2 on the Crystal Structure Stability of SFC at 1473 K (1200 A degrees C). *Metall. Mater. Trans. B-Process Metall. Mater. Proc. Sci.* **2015**, *46*, 1146–1153, doi:10.1007/s11663-015-0313-2.
12. Murakami, T.; Kodaira, T.; Kasai, E. Effect of the Reduction of Calcium Ferrite on Disintegration Behavior of Sinter under High Hydrogen Atmosphere. *ISIJ Int.* **2015**, *55*, 1197–1205, doi:10.2355/isijinternational.55.1197.
13. Hessien, M.M.; Kashiwaya, Y.; Ishii, K.; Nasr, M.I.; El-Geassy, A.A. Sintering and heating reduction processes of alumina containing iron ore samples. *Ironmak. Steelmak.* **2008**, *35*, 191–204, doi:10.1179/174328107x174663.
14. Ying, Z.W.; Xu, L.X.; Jiang, M.F.; Shen, Y.S. Effect of Calcium Ferrite Morphology on Anti-Fracture Ability of Sinters. *J. Iron Steel Res. Int.* **2006**, *18*, 55–58, doi:10.3321/j.issn:1001-0963.2006.02.013.
15. Hida, Y.; Okazaki, J.; Itoh, K.; Sasaki, M. Formation Mechanism of Acicular Calcium Ferrite of Iron Ore Sinter (Sinter). *Tetsu Hagane* **1987**, *73*, 1893–1900, doi:10.2355/tetsutohagane1955.73.15_1893.
16. Cai, B.; Watanabe, T.; Kamijo, C.; Susa, M.; Hayashi, M. Comparison between Reducibilities of Columnar Silico-ferrite of Calcium and Aluminum (SFCA) Covered with Slag and Acicular SFCA with Fine Pores. *ISIJ Int.* **2018**, *58*, 642–651, doi:10.2355/isijinternational.ISIJINT-2017-552.
17. Ding, C.; Lv, X.; Xuan, S.; Qiu, J.; Chen, Y.; Bai, C. Effect of Silica on Reduction of Calcium Ferrite with CO-N-2 Gas Mixtures. *ISIJ Int.* **2017**, *57*, 634–642, doi:10.2355/isijinternational.ISIJINT-2016-441.
18. Xuan, S.; Lv, X.; Ding, C.; Tang, K.; Li, G.; Pei, G.; Wu, S. Reduction Behavior of Aluminate Calcium Ferrite (CFA) in CO-N-2 Atmosphere. *Steel Res. Int.* **2018**, *89*, 1700452, doi:10.1002/srin.201700452.
19. Marshall, D.B.; Tatsuo, N.; Evans, A.C. A simpled method for determining elastic modulus to hardness ratios using Knoop indentation measurements. *J. Am. Ceram. Soc.* **1982**, *65*, 175–176, doi:10.1111/j.1151-2916.1982.tb10357.x.
20. Wang, G.; Zhang, J.; Hou, X.; Shao, J.; Geng, W. Study on CO_2 gasification properties and kinetics of biomass chars and anthracite char. *Bioresour. Technol.* **2015**, *177*, 66–73, doi:10.1016/j.biortech.2014.11.063.
21. Wang, G.; Zhang, J.; Shao, J.; Ren, S. Characterisation and model fitting kinetic analysis of coal/biomass co-combustion. *Thermochim. Acta* **2014**, *591*, 68–74, doi:10.1016/j.tca.2014.07.019.
22. Xu, R.; Zhang, J.; Wang, G.; Zuo, H.; Li, P.; Wang, H.; Lin, H.; Liu, S. Isothermal kinetic analysis on fast pyrolysis of lump coal used in COREX process. *J. Therm. Anal. Calorim.* **2016**, *123*, 773–783, doi:10.1007/s10973-015-4972-7.
23. Xu, R.; Dai, B.; Wang, W.; Schenk, J.; Xue, Z. Effect of iron ore type on the thermal behaviour and kinetics of coal-iron ore briquettes during coking. *Fuel Proc. Technol.* **2018**, *173*, 11–20, doi:10.1016/j.fuproc.2018.01.006.
24. Xu, R.; Zheng, H.; Wang, W.; Schenk, J.; Xue, Z. Influence of Iron Minerals on the Volume, Strength, and CO2 Gasification of Ferro-coke. *Energy Fuels* **2018**, doi:10.1021/acs.energyfuels.8b02644.
25. Zheng, H.; Wang, W.; Xu, R.; Zan, R.; Schenk, J.; Xue, Z. Effect of the particle size of iron ore on the pyrolysis kinetic behaviour of coal-iron ore briquettes. *Energies* **2018**, *11*, 2595, doi:10.3390/en11102595.
26. Xu, R.; Wang, W.; Dai, B. Influence of particle size on the combustion behaviors of bamboo char used for blast furnace injection. *J. Iron Steel Res. Int.* **2018**, *25*, 1213–1222, doi:10.1007/s42243-018-0186-0.
27. Wang, G.; Zhang, J.; Zhang, G.; Wang, H.; Zhao, D. Experiments and Kinetic Modeling for Reduction of Ferric Oxide-biochar Composite Pellets. *ISIJ Int.* **2017**, *57*, 1374–1383, doi:10.2355/isijinternational.ISIJINT-2016-630.